nature COMMUNICATIONS

ARTICLE

https://doi.org/10.1038/s41467-022-31503-0 OPEN

Unveiling the S=3/2 Kitaev honeycomb spin liquids

Hui-Ke Jin[1]✉, W. M. H. Natori[2,3], F. Pollmann[4,5] & J. Knolle[1,3,5]

The S=3/2 Kitaev honeycomb model (KHM) is a quantum spin liquid (QSL) state coupled to a static Z_2 gauge field. Employing an SO(6) Majorana representation of spin3/2's, we find an exact representation of the conserved plaquette fluxes in terms of static Z_2 gauge fields akin to the S=1/2 KHM which enables us to treat the remaining interacting matter fermion sector in a parton mean-field theory. We uncover a ground-state phase diagram consisting of gapped and gapless QSLs. Our parton description is in quantitative agreement with numerical simulations, and is furthermore corroborated by the addition of a [001] single ion anisotropy (SIA) which continuously connects the gapless Dirac QSL of our model with that of the S=1/2 KHM. In the presence of a weak [111] SIA, we discuss an emergent chiral QSL within a perturbation theory.

[1] Department of Physics TQM, Technische Universität München, James-Franck-Straße 1, D-85748 Garching, Germany. [2] Institute Laue-Langevin, BP 156, 41 Avenue des Martyrs, 38042 Grenoble, Cedex 9, France. [3] Blackett Laboratory, Imperial College London, London SW7 2AZ, UK. [4] Department of Physics CMT, Technische Universität München, James-Franck-Straße 1, D-85748 Garching, Germany. [5] Munich Center for Quantum Science and Technology (MCQST), 80799 Munich, Germany. ✉email: huike.jin@tum.de

The search for quantum spin liquids (QSLs) has been at the forefront of condensed matter physics for many decades because they represent novel quantum phases of matter beyond the Landau paradigm of symmetry breaking—instead they are characterized by fractionalized excitations and non-local quantum entanglement[1–4]. A paradigmatic example of a two-dimensional (2D) QSL is the seminal Kitaev honeycomb model (KHM)[5], which was initially derived to illustrate the basic ideas of topological quantum computation[6]. Remarkably, the model has an exact solution which shows that its excitations are free Majorana fermions with a Dirac dispersion and gapped conserved plaquette fluxes which couple to the Majoranas via a *static* Z_2 gauge field. In the context of frustrated magnetism research, the KHM provided a first rigorous example how a QSL with fractionalized excitations and emergent gauge fields can emerge in a concrete microscopic 2D spin model.

In the last years, the KHM has transformed from a theoretical toy model to one of experimental relevance because a flurry of spin-orbit-coupled 4*d* and 5*d* transition metal compounds[7–12] has been proposed as candidates for realizing its bond-anisotropic Ising interactions. Remarkably, experiments have also observed signatures of the proximate Kitaev spin liquid (KSL) in several materials with effective spin 1/2 moments, such as α-$RuCl_3$[13–18] and $(Na_{1-x}Li_x)_2IrO_3$[19,20], despite the residual zigzag ordered state which appears at low temperature[21,22] because of additional interactions, e.g., an off-diagonal symmetric Γ exchange[13]. However, the exchange frustration of the KHM is not restricted to spin 1/2 and recently some promising realizations of higher-spin Kitaev materials have been proposed based upon 3*d* orbitals[23–25], in which the QSL-disrupting non-Kitaev exchanges might be reduced[26–28]. In particular, a microscopic derivation of the S=3/2 KHM model with an extra single ion anisotropy (SIA) has been established for the quasi 2D systems CrI_3 and $CrGeTe_3$[23,24].

After the original proposal of the S=1/2 KHM[5], much effort has been devoted to investigating the KHM models for S > 1/2, which have not found an exact solution[29–36]. Nevertheless, Baskaran et al.[30] showed early on that a generic spin-S KHM still has conserved Z_2 fluxes for each elementary hexagon and suggested via a semiclassical analysis that the ground state of KHMs for all values of S exhibits a homogeneous flux configuration in which all values of Z_2 fluxes are $+1$[30]. Subsequently, it has been proposed that the ground states of the S > 3/2 KHMs are Z_2 QSLs described by an effective toric code on a honeycomb superlattice, but the employed semi-classical analysis breaks down precisely at S=3/2[34]. The S=1 KHM is amenable to numerical investigations and studies using exact diagonalization[33] and density matrix renormalization group (DMRG)[35] point to a gapless QSL ground state, whereas a tensor network approach proposes a gapped QSL for the isotropic model[36]. Overall, the S=3/2 KHM seems to be the least understood of all Kitaev models — the conserved plaquette fluxes alone do not help to gain an analytical understanding and a high density of low energy excitations lead to strong finite-size effects for numerical investigations.

Here, we report new exact properties of the S=3/2 KHM and provide a systematic understanding of its ground-state phase diagram and excitations. We introduce an SO(6) Majorana representation for the spin-3/2's which permits an exact mapping of the spin model to one of fermions coupled to a *static* Z_2 gauge field. The latter determines the conserved plaquette flux just like in the original S=1/2 KHM. Within a given gauge field configuration, the Hamiltonian still contains quartic and even sextic fermion interaction terms but we construct a parton mean-field (MF) theory which turns out to be even quantitatively reliable. Our theory is furthermore corroborated by the addition of an extra [001] SIA to the S=3/2 KHM, which still preserves the conservation of the Z_2 fluxes and allows us to map out the phase diagram consisting of two gapless Dirac and two gapped QSLs. In the limit of large [001] SIA, we find an exact solution of an effective S=1/2 KSL, which is continuously connected to one of the two gapless phases of the pure S=3/2 KHM. We also investigate the model using DMRG[37,38] and find the numerical results to be in quantitative agreement with the predictions from our parton MF theory. In the presence of a weak [111] SIA, we can derive an effective Hamiltonian within the zero-flux sector and argue that a chiral KSL is established.

Results

Model Hamiltonian. The Hamiltonian of the S=3/2 KHM reads

$$\mathcal{H} = \sum_{\langle ij\rangle_a} J_a S_i^a S_j^a, \tag{1}$$

where S_i^a $(a = x, y, z)$ are three components of an S=3/2 spin at site i and $\langle ij\rangle_a$ denotes the nearest neighbor (NN) bonds of a-type S=3/2 Ising interactions (see Fig. 1). There exist commuting plaquette operators W_p for each hexagon p (see Fig. 1) as $W_p \equiv -e^{i\pi(S_1^x+S_2^y+S_3^z+S_4^x+S_5^y+S_6^z)}$[30]. By noticing that $[W_p, \mathcal{H}] = 0$, the total Hilbert space of Hamiltonian (1) can be divided into orthogonal sectors characterized by flux configurations $\{w_p = \pm 1\}$, where w_p is the eigenvalue of W_p.

SO(6) Majorana representation. We introduce three gauge Majorana fermions η_i^a and three itinerant Majorana fermions $\theta_i^a (a = x, y, z)$, to obtain the SO(6) Majorana representation for spin-3/2's[39–52]: $S_i^a = \frac{i}{4}\epsilon_{abc}\eta_i^b\eta_i^c - \frac{i}{2}\eta_i^a\tilde{\theta}_i^a$, where $\tilde{\theta}_i^{x(y)} = \theta_i^z - (+)\sqrt{3}\theta_i^x$, $\tilde{\theta}_i^z = -2\theta_i^z$, and ϵ_{abc} is the Levi-Civita tensor (summation over repeated indices throughout). This parton representation doubly enlarges the Hilbert space and the physical Hilbert space of spin-3/2's can be restored by imposing the local constraint $D_i = i\eta_i^x\eta_i^y\eta_i^z\theta_i^x\theta_i^y\theta_i^z = 1$. One can then obtain $i\eta_i^b\eta_i^c = \epsilon_{abc}\eta_i^a\theta_i^x\theta_i^y\theta_i^z$ and rewrite the spin operators as

$$S_i^a = \frac{i}{2}\eta_i^a\left(\theta_i^{xyz} - \tilde{\theta}_i^a\right), (a = x, y, z), \tag{2}$$

where $\theta_i^{xyz} = -i\theta_i^x\theta_i^y\theta_i^z$.

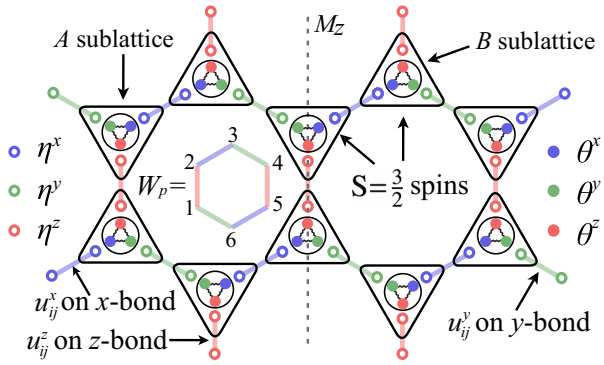

Fig. 1 Graphic representation of the S=3/2 KHM (3) and the SO(6) Majorana representation. Down (up) triangles stand for S=3/2 spins on *A* (*B*) sublattice. Each spin is represented by SO(6) Majoranas, e.g., three gauge Majoranas $\eta^{x,y,z}$ (circles) and three itinerant Majoranas $\theta^{x,y,z}$ (dots). The blue, green, and red bold lines denote the *static* Z_2 gauge fields u^x, u^y, and u^z for *x*-, *y*-, and *z*-bond Ising interactions, respectively. The plaquette operator $W_p \equiv -e^{i\pi(S_1^x+S_2^y+S_3^z+S_4^x+S_5^y+S_6^z)}$ can be expressed as the product of u_{ij}^a around hexagon *p*. The gray dashed line stands for the mirror symmetry M_z with $J_x = J_y$.

Eq. (1) then becomes an effective Hamiltonian for Majoranas

$$H = -\frac{i}{4}\sum_{\langle ij\rangle_a} J_a u_{ij}^a \left(\theta_i^{xyz} - \tilde{\theta}_i^a\right)\left(\theta_j^{xyz} - \tilde{\theta}_j^a\right), \tag{3}$$

where $u_{ij}^a = i\eta_i^a \eta_j^a$. One can now verify that $[u_{ij}^a, u_{kl}^b] = 0$ for all different bonds and $[u_{ij}^a, H] = 0$. Therefore, u_{ij}^a with eigenvalues ± 1 is a *static* Z_2 gauge field! Similar to the S=1/2 KHM, the plaquette operator W_p is exactly mapped to a product of u_{ij}^a around hexagon p, e.g., $W_p = u_{12}^z u_{32}^x u_{34}^y u_{54}^z u_{56}^x u_{16}^y$ (see Fig. 1). In a fixed Z_2 gauge field configuration the Hamiltonian only depends on the itinerant Majoranas θ_i^a.

The microscopic derivation of the S=3/2 KHM introduced in Ref. [23–25] suggests that it is usually accompanied by an extra [111] SIA term of the form $\left(S_i^c\right)^2$ with $S_i^c = \frac{1}{\sqrt{3}}\left(S_i^x + S_i^y + S_i^z\right)$. In addition to the [111] SIA, we also consider a simplified [001] SIA term and focus on the Hamiltonian

$$\mathcal{H}_D = \mathcal{H} + \sum_i \left[D_z (S_i^z)^2 + D_c \left(S_i^c\right)^2\right]. \tag{4}$$

Note that $[W_p, \sum_i \left(S_i^z\right)^2] = 0$ but the [111] SIA breaks the conservation of fluxes, namely, $[W_p, \sum_i \left(S_i^c\right)^2] \neq 0$. Therefore we always treat D_c as a small perturbation to ensure that the system is close to the Kitaev limit.

The [001] SIA limit. First, we focus on the $D_c = 0$ limit with conserved fluxes. Since the local S=3/2 states of $\left|S_i^z = \pm\frac{3}{2}\right\rangle$ $\left(\left|S_i^z = \pm\frac{1}{2}\right\rangle\right)$ will be energetically favored when J_z (D_z) dominates, we expect that the competition of J_z and D_z leads to a rich phase diagram. Moreover, below we show that for $D_z \to \infty$, we can recover an effective S=1/2 KSL.

By using $\left(S_i^z\right)^2 = -i\theta_i^x\theta_i^y$ (a constant of 5/4 has been omitted), the effective Majorana Hamiltonian can be divided into two parts. One is a quadratic Hamiltonian $H^{(2)}(\{u\}) \equiv \frac{-i}{4}\sum_{\langle ij\rangle_a} J_a u_{ij}^a \tilde{\theta}_i^a \tilde{\theta}_j^a - iD_z \sum_i \theta_i^x \theta_i^y$, and the other is an interacting Hamiltonian consisting of quartic and sextic terms, which we treat within a MF analysis. In our decoupling scheme, the MF Hamiltonian reads

$$\begin{aligned} H_{\mathrm{MF}}(\{u\}) = H^{(2)}(\{u\}) + \sum_{\langle ij\rangle_a} \frac{iJ_a u_{ij}^a}{4}\Big\{ & \frac{\epsilon_{opq}\epsilon_{rst}}{4}\langle\theta_i^o\theta_i^p\theta_j^r\theta_j^s\rangle\theta_i^q\theta_j^t \\ & + \frac{\epsilon_{lmn}}{2}\left(\theta_i^m\theta_i^n\langle\theta_i^l\theta_j^x\theta_j^y\theta_j^z\rangle - \theta_j^m\theta_j^n\langle\theta_j^l\theta_i^x\theta_i^y\theta_i^z\rangle\right) \\ & + \frac{\epsilon_{uvw}}{2}\left[\left(Q_i^{uv}\theta_i^w\tilde{\theta}_j^a - \Delta_{ij}^{w\tilde{a}}\theta_i^u\theta_i^v + iQ_i^{uv}\Delta_{ij}^{w\tilde{a}}\right) - (i \leftrightarrow j)\right]\Big\} \end{aligned} \tag{5}$$

with the on-site parameters $Q_i^{ab} \equiv -\langle i\theta_i^a\theta_i^b\rangle$ $(a \neq b)$ and bond parameters $\Delta_{ij}^{ab} \equiv \langle i\theta_i^a\theta_j^b\rangle$ $\left(\Delta_{ij}^{a\tilde{b}} \equiv \langle i\theta_i^a\tilde{\theta}_j^b\rangle\right)$. In accordance with Wick's theorem, the average of quartic terms can be decoupled as $\langle\theta_i^o\theta_i^p\theta_j^r\theta_j^s\rangle = -Q_i^{op}Q_j^{rs} + \Delta_{ij}^{or}\Delta_{ij}^{ps} - \Delta_{ij}^{os}\Delta_{ij}^{pr}$ and $\langle\theta_i^l\theta_j^x\theta_j^y\theta_j^z\rangle = \Delta_{ij}^{lx}Q_j^{yz} + \Delta_{ij}^{ly}Q_j^{zx} + \Delta_{ij}^{lz}Q_j^{xy}$. Eventually, H_{MF} is parameterized by MF parameters Q and Δ, which we determine self-consistently (see Supplementary Note 1). In the presence of Z_2 flux conservation, we can restrict to antiferromagnetic couplings of $J_a > 0$ since in the parton level a sign change of $J_a \to -J_a$ can be resolved by $u_{ij}^a \to -u_{ij}^a$. For simplicity, we focus on the case of $J_x = J_y = 1$ with a mirror symmetry M_z across the z-bonds (see Fig. 1) which leads to a vanishing of $Q^{yz,zx} = 0$. The only nonzero on-site parameter is $Q^{xy} \equiv -\langle i\theta^x\theta^y\rangle = \langle(S^z)^2\rangle$ which is a time-reversal-invariant spin quadrupolar component characterizing the MF ground states of $H_{\mathrm{MF}}(\{u\})$ (see Supplementary Note 2).

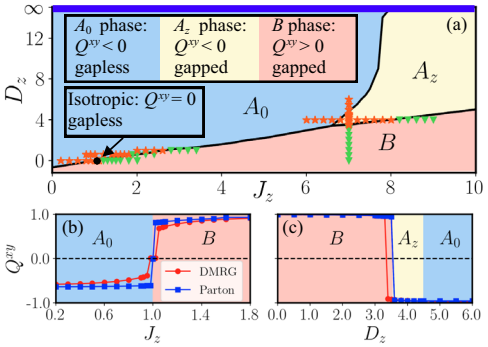

Fig. 2 The ground-state phase diagram and the values of parameter Q^{xy}. **a** The MF phase diagram of Hamiltonian (5) in zero-flux sector on a 36 × 36 torus. The A_0 phase is a Dirac QSL with spin quadrupolar parameter $Q^{xy} < 0$. In the A_z (B) phase, the Majorana excitations are gapped with $Q^{xy} < 0$ ($Q^{xy} > 0$). At the isotropic point, the ground state is a QSL with $Q^{xy} = 0$. The bold blue line at $D_z = \infty$ with $J_z < 8$ ($J_z > 8$) represents the effective gapless (gapped) S=1/2 KSL. The gapless phases in S=3/2 and S=1/2 KHMs can continuously connect to each other through the A_0 phase without energy gap opening. The orange stars (green triangles) represent the ground states obtained by DMRG on a 3 × 4 torus with zero-flux (disordered-flux) configurations with bond dimension $\chi = 4000$. The values of Q^{xy} as a function of J_z with $D_z = 0$ (**b**) and D_z with $J_z = 7$ (**c**). The computations of DMRG and parton MF theory are performed on a 3 × 4 torus.

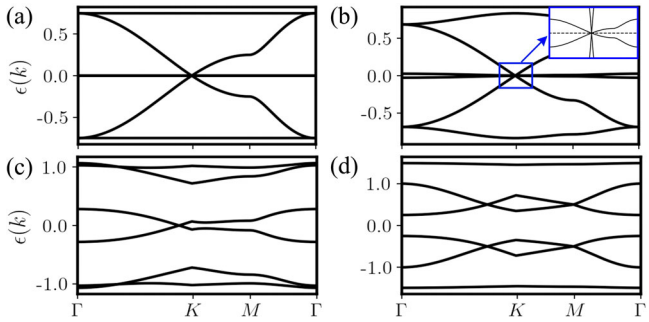

Fig. 3 Band structure of itinerant Majorana fermions. a The Majorana band structure of the quadratic Hamiltonian $H^{(2)}$ at the isotropic point $J_z = 1$ and $D_z = 0$. The Majorana band structures of the MF Hamiltonian H_{MF} with (**b**) $J_z = 1$ and $D_z = 0$, (**c**) $J_z = 1.2$ and $D_z = 0.4$, and (**d**) $J_z = 1.4$ and $D_z = 0$. Here $J_x = J_y = 1$, and a zero-flux configuration of $\{u\} = 1$ is used. The inset in (**b**) shows the zoom-in around the K point.

Following the proposal of Ref. [30] that for generic spin-S KHMs the ground-state always exhibits a zero-flux configuration with $\{w_p\} = 1$, we will mainly focus on the zero-flux sector and fix $\{u\} = 1$ for studying the Majorana excitations of H_{MF}. Note that the quadratic Hamiltonian $H^{(2)}(\{u\})$ alone always energetically favors a zero-flux state.

The Hamiltonian $H_{\mathrm{MF}}(\{u\} = 1)$ displays four phases which are characterized by their distinct Majorana excitations and the value of the quadrupolar parameter Q^{xy}, as shown in Fig. 2a. (i) At the isotropic point of $J_z = 1$ and $D_z = 0$, the ground state is a Dirac QSL with $Q^{xy} = 0$. The Majorana band structure of $H_{\mathrm{MF}}(\{u\} = 1)$ at the isotropic point is almost the same as that of the quadratic Hamiltonian $H^{(2)}(\{u\} = 1)$, except that the exact flat bands populated by θ^y in Fig. 3a acquire a very narrow dispersion as shown in Fig. 3b. Consequently, in this phase $H_{\mathrm{MF}}(\{u\} = 1)$ has a Dirac point at the K-point, around which there exist two gapless Majorana bands crossing linearly at zero energy but one of whose velocity is close to zero. (ii) In the A_0 phase, the ground state is a

Dirac QSL coexisting with a spin quadrupolar parameter $Q^{xy} < 0$. Because of a nonzero $Q^{xy} < 0$, only one branch of gapless spin excitations remains around the Dirac point (see Fig. 3c). (iii) In the A_z phase, the effect of D_z remains, but a relatively large anisotropy of J_z gaps out all Majorana excitations and the ground state is a gapped QSL coexisting with a spin quadrupolar parameter $Q^{xy} < 0$. (iv) In the B phase, the dominant J_z leads to a positive $Q^{xy} > 0$ and all Majorana excitations are gapped. Fig. 3d shows a typical Majorana band structure for the B phase. We conclude that the transition between the B phase and the A_0 (A_z) phase is of first-order since Q^{xy} shows a discontinuous bump at the phase boundary in Fig. 2b, c.

Effective S=1/2 KSL. A key advantage of using the [001] SIA is that the Hamiltonian can be solved exactly in the limit of $D_z \to \infty$, because the high energy local states of $\left|S_i^z = \pm\frac{3}{2}\right\rangle$ are removed and the ground-state subspace of Hamiltonian (4) is spanned by the local states of $\left|S_i^z = \pm 1/2\right\rangle$ only. Within the framework of the SO(6) Majorana representation, the itinerant Majoranas θ_i^x and θ_i^y are paired up subjected to the constraint $i\theta_i^x\theta_i^y = 1$ ($Q^{xy} = -1$). Then the three S=3/2 operators in Eq. (2) projected onto the subspace of $i\theta_i^x\theta_i^y = 1$ become

$$S_i^z \simeq \frac{i}{2}\eta_i^z\theta_i^z, \qquad S_i^{x(y)} \simeq i\eta_i^{x(y)}\theta_i^z. \tag{6}$$

Obviously, Eq. (6) is equivalent to Kitaev's original four-Majorana representation[5]. It is remarkable that an effective S=1/2 KHM with a renormalized coupling constant $J_z \to J_z/4$ emerges in our S=3/2 Hamiltonian (3) for $D_z \to \infty$ with an effective gapless (gapped) S=1/2 KSL for $J_z < (>)8$. This connection gives additional support to the assumption of a zero-flux ground state and our MF treatment, which is known to exactly capture the phase diagram and nature of excitations of the S=1/2 KHM[53,54]. Indeed, we find that the gapless KSL of the emergent S=1/2 KHM is continuously connected to the gapless A_0 phase of the pure S=3/2 KHM in Fig. 2a.

Numerical results. Since Lieb's theorem[55] may not be applicable for the interacting Hamiltonian (3), we examine the zero-flux ground-state configuration, which is a pivotal assumption in our parton theory. We find that the ground states in our DMRG simulations always exhibit a zero-flux configuration in the A_0 and A_z phases. In contrast, for the B phase, DMRG does not converge to a unique ground-state flux configuration but instead leads to a disordered-flux ground state in which the measured flux for each plaquette is neither 1 nor −1. The data points for different DMRG-obtained ground-state flux configurations are shown in Fig. 2a.

The disordered-flux ground states obtained by DMRG indicate an extremely small flux gap above the zero-flux state in the B phase. This flux gap can also be evaluated within our MF theory in the B phase. To connect to our DMRG simulations, we have performed the MF calculations on the same 3×4 torus. We find that the energy of a pair of neighboring fluxes is $E_{2\text{fluxes}} \simeq 10^{-6}$ for $J_z = 1.2$ and $D_z = 0$, which is as small as the corresponding DMRG truncation error $\epsilon \simeq 10^{-6}$. The flux gap $E_{2\text{fluxes}}$ rapidly decreases as J_z increases, which explains why DMRG fails to capture the conserved Z_2 flux in the B phase.

Next, we investigate the local spin quadrupolar parameter Q_i^{xy} using DMRG and find that the Q_i^{xy} are spatially uniform (on the torus and in the bulk of cylinders) as assumed in our parton description. A remarkable observation is that, if we ignore small discrepancies near the phase boundaries, the values of the DMRG-obtained Q^{xy} are even in quantitative agreement with those given by the parton MF theory within the zero-flux sector,

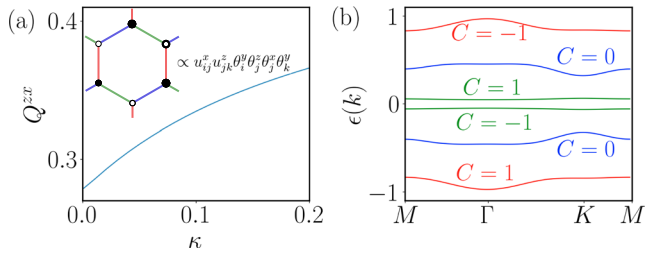

Fig. 4 Chiral KSL induced by [111] SIA. a Q^{zx} as a function of κ. Inset: A sketch for the three-body quadrupolar interactions in Eq. (7). The blue, green, and red bonds stand for the x-, y-, and z-type S=3/2 Ising interactions, respectively. The summation in Eq. (7) takes place over the triangle with vertexes i, j, and k (and symmetry-equivalent ones). **b** The band structure and corresponding Chern numbers for the parton MF theory in Eq. (8) with $\kappa = 0.01$.

as shown in Fig. 2b, c. For the purpose of comparison, we have chosen the same lattice geometry, e.g., a 3×4 torus, to calculate the MF and DMRG values of Q^{xy}. The difference between the MF Q^{xy} for a 3×4 torus and its extrapolation to an infinite lattice is of the magnitude of 10^{-2} (except near the phase boundaries), thus finite-size effects for Q^{xy} are small. This remarkable quantitative agreement demonstrates that our SO(6) Majorana MF theory provides a compelling scenario for describing the S=3/2 KHM. For example, we can now understand why the S=3/2 KHM at the isotropic point is so challenging for numerical methods, e.g., the extreme system-size dependence encountered in our DMRG simulations, because the almost flat Majorana bands, see Fig. 3b, lead to a large pile up of close to zero energy states.

The [111] SIA limit. Next, we study the experimentally more relevant case, i.e., $J_x = J_y = J_z = J$, $D_z = 0$, and $D_c \ll |J|$. A finite [111] SIA breaks the flux conservation, leading to a dynamical gauge field. In analogy to the procedure of treating a magnetic field in the S=1/2 KHM[5], we circumvent this problem by deriving an effective three-body quadrupolar interaction within the zero-flux sector. This can be further motivated by noticing that $\left(S_i^c\right)^2 = -\frac{i}{3}\left(\eta_i^x + \eta_i^y + \eta_i^z\right)\theta_i^y$ plays a similar role as the [111] magnetic field in the $S = 1/2$ KHM[5]. The effective term $H^{(3)}$ described by three-body quadrupolar interactions is represented by

$$H^{(3)} = \kappa \sum_{\langle ij\rangle_a \langle jk\rangle_b} u_{ij}^a u_{jk}^b \left(i\theta_i^y\theta_j^z\right)\left(i\theta_j^x\theta_k^y\right), \tag{7}$$

where $\kappa \sim D_c^3/\Delta_{\text{flux}}^2$ ($\Delta_{\text{flux}} \approx 0.093J$) and $\langle ij\rangle_\alpha$ and $\langle ij\rangle_\beta$ are two NN bonds connected by site j (see Fig. 4a). Eq. (7) clearly commutes with the Z_2 gauge fields but is quartic in the itinerant Majoranas. Its most general decoupling reads

$$\begin{aligned} H_{\text{MF}}^{(3)}(\{u\} = 1) = \kappa \sum_{\langle ij\rangle_a \langle jk\rangle_b} & i\left(\Delta_{ij}^{yz}\theta_j^x\theta_k^y + \Delta_{kj}^{yx}\theta_j^z\theta_i^y\right) \\ + \kappa \sum_{\langle ij\rangle_a \langle jk\rangle_b} & i\left(-Q_j^{zx}\theta_i^y\theta_k^y + \xi_{ik}^{yy}\theta_j^x\theta_j^y\right), \end{aligned} \tag{8}$$

where $\xi_{ik}^{yy} = -\langle i\theta_i^y\theta_k^y\rangle$ is the hopping parameter on the 2nd NN bond. A nonzero Q^{zx} breaks time-reversal symmetry (TRS) so that $H_{\text{MF}}^{(3)}$ naturally describes a chiral KSL analogous to the $S = 1/2$ case[5]. A key difference is that here TRS is *spontaneously* broken since Eqs. (4) and (7) are even under time-reversal.

$H_{\text{MF}}^{(3)}$ favors the $S = 3/2$ chiral KSL, which undergoes a first-order phase transition on the parton MF level. For small $\kappa = 0.01$, the self-consistent solution converges to parameters $Q^{zx} \approx 0.28$ and $|\xi^{yy}| \approx 0.115$. Fig. 4a presents the evolution of Q^{zx} as a

function of positive κ—solutions for negative κ are obtained by changing the signs of Q^{zx}, ξ^{yy}, and $\Delta^{yx(z)}$.

Next, we study properties of this chiral KSL. The Majorana hybridization induced by a nonzero Q^{zx} narrows all dispersions and separates the six bands from each other, see Fig. 4b. We evaluate the topological characteristics of these bands in terms of the Chern number, which is

$$C's = (1, 0, -1, 1, 0, -1)$$

for the lowest to the highest band. Notice that in contrast to the $S = 1/2$ chiral KSL, the sum of Chern numbers over the negative energy bands is zero. Therefore, no quantized thermal Hall conductivity is expected in the low temperature limit, but an activated signal emerges for increasing temperatures.

Discussion

In summary, we have studied the ground-state phase diagram and excitations of the S=3/2 KHM with additional SIA terms. We employed a parton theory based on the SO(6) Majorana representation of spin=3/2's, which is supported by DMRG simulations. We have shown that the conserved flux for each honeycomb plaquette can be represented exactly via a static Z_2 gauge field similar to the well-known S=1/2 KHM, which is key for identifying the correct MF decoupling of the parton description. For a [001] SIA, DMRG calculations are shown to agree with our self-consistent MF theory qualitatively and even quantitatively. We uncover a rich phase diagram characterized by distinct Majorana excitations and different phases with spin quadrupolar parameter $Q^{xy} = \langle (S^z)^2 \rangle$: (i) a gapless Dirac QSL with $Q^{xy} = 0$ and an additional almost flat Majorana band close to zero energy at the isotropic point ($J_z = 1, D_z = 0$); (ii) a gapless Dirac QSL with $Q^{xy} < 0$ in the A_0 phase; (iii) a gapped QSL with $Q^{xy} < 0$ in the A_z phase; and (iv) a gapped QSL with $Q^{xy} > 0$ in the B phase. For a dominating [001] SIA, the low energy sector of the S=3/2s reduces to effective S=1/2s which allows us to continuously connect the gapless A_0 phase of the pure S=3/2 KHM to that of the well-known Dirac QSL of the S=1/2 KHM. In the B phase, we found that DMRG fails to capture the conservation of Z_2 fluxes because of an extremely small flux gap above the zero-flux ground state, which is again accounted for in our parton MF theory. In the presence of a small [111] SIA, we establish an effective model in the zero-flux sector with three-body quadrupolar interactions. Our parton MF study indicates an emergent chiral KSL spontaneously breaking TRS.

We argue that our SO(6) Majorana parton theory efficiently describes the different QSLs of the S=3/2 KHM, which also provides a compelling scenario for explaining the difficulties encountered in the numerical studies. Hence, it will provide an good starting point for studying the robustness of the QSL regimes with respect to additional terms in the Hamiltonian, for example different exchange interactions and the SIA relevant for microscopic realizations of the S=3/2 KHM[24]. The connection to the S=1/2 KHM indicates that in particular the ferromagnetic QSLs will be very fragile and, in general, the formation of conventional magnetic order will be further facilitated because of flux-fermion bound state formation involving the almost flat Majorana bands. In that context, large-scale numerical studies for S=3/2 KHM with non-Kitaev interactions like [111] SIA and Heisenberg terms are still highly demanded, and the quality of our parton MF states can be further improved by efficient tensor network representation with Gutzwiller projection[56–58] or by including different flux sectors in the variational ansatz[59].

In the future, it will be worthwhile to study the effect of applying a magnetic field and the ensuing QSL phases of the S=3/2 KHM. Similarly, it would be desirable to generalize our Majorana parton construction to higher-spin systems whose dimension of local Hilbert space is 2^n (with n integer), i.e., the S=7/2 KHM could possibly have a similar exact static Z_2 gauge field permitting an efficient description via an eight Majorana representation for spin-7/2's.

Methods

In order to examine the reliability of our parton MF theory in the case of a [001] SIA, we employ state-of-the-art DMRG method[37,38] to study the ground state of Hamiltonian (4). DMRG is a very powerful numerical approach for studying 1D strongly-correlated systems. To perform DMRG calculations on a 2D honeycomb lattice of $L_1 \times L_2$ unit cells, we consider a cylindrical geometry for which the periodic boundary condition (PBC) is imposed along the shorter direction (e.g., the circumference L_1), while the longer (e.g., the length L_2) is left open. Moreover, we also adopt small tori with PBCs along both directions to strictly preserve the A/B sublattice and translational symmetries. The DMRG simulations are performed on a 3×4 torus as well as a 4×8 cylinder ($L_1 = 4$). The bond dimension of DMRG is kept as large as $\chi = 4000$, resulting in a typical truncation error of $\epsilon \simeq 10^{-6}$ ($\epsilon \simeq 10^{-4}$ close to the isotropic point $J_z = 1$ and $D_z = D_c = 0$). In general, we encounter significant finite-size effects in our numerical studies in contrast to checks on the S=1/2 and S=1 KHMs.

Data availability

All data needed to evaluate the conclusions in the paper are present in the paper and/or the Supplementary Information. The raw data sets used for the presented analysis within the current study are available from the corresponding authors on reasonable request.

Code availability

The code that support the findings of this study is available from the corresponding author upon reasonable request.

Received: 19 November 2021; Accepted: 16 June 2022;
Published online: 02 July 2022

References

1. Broholm, C. et al. Quantum spin liquids. *Science* **367**, eaay0668 (2020).
2. Knolle, J. & Moessner, R. A field guide to spin liquids. *Ann. Rev. Cond. Matter Phys.* **10**, 451–472 (2019).
3. Zhou, Y., Kanoda, K. & Ng, T.-K. Quantum spin liquid states. *Rev. Mod. Phys.* **89**, 025003 (2017).
4. Savary, L. & Balents, L. Quantum spin liquids: a review. *Rep. Progr. Phys.* **80**, 016502 (2016).
5. Kitaev, A. Anyons in an exactly solved model and beyond. *Ann. Phys.* **321**, 2–111 (2006).
6. Nayak, C., Simon, S. H., Stern, A., Freedman, M. & Das Sarma, S. Non-abelian anyons and topological quantum computation. *Rev. Mod. Phys.* **80**, 1083–1159 (2008).
7. Jackeli, G. & Khaliullin, G. Mott insulators in the strong spin-orbit coupling limit: from Heisenberg to a quantum compass and Kitaev models. *Phys. Rev. Lett.* **102**, 017205 (2009).
8. Chaloupka, Jcv, Jackeli, G. & Khaliullin, G. Kitaev-Heisenberg model on a honeycomb lattice: Possible exotic phases in iridium oxides A_2iro$_3$. *Phys. Rev. Lett.* **105**, 027204 (2010).
9. Rau, J. G., Lee, E. K.-H. & Kee, H.-Y. Spin-orbit physics giving rise to novel phases in correlated systems: Iridates and related materials. *Ann. Rev. Cond. Matter Phys.* **7**, 195–221 (2016).
10. Trebst, S. & Hickey, C. Kitaev materials. *Phys. Rep.* **950**, 1–37 (2022).
11. Hermanns, M., Kimchi, I. & Knolle, J. Physics of the Kitaev model: fractionalization, dynamical correlations, and material connections. *Ann. Rev. Cond. Matter Phys.* **9**, 17–33 (2018).
12. Takagi, H., Takayama, T., Jackeli, G., Khaliullin, G. & Nagler, S. E. Concept and realization of Kitaev quantum spin liquids. *Nat. Rev. Phys.* **1**, 264–280 (2019).
13. Plumb, K. W. et al. $\alpha - RuCl_3$: A spin-orbit assisted Mott insulator on a honeycomb lattice. *Phys. Rev. B* **90**, 041112 (2014).
14. Sandilands, L. J., Tian, Y., Plumb, K. W., Kim, Y.-J. & Burch, K. S. Scattering continuum and possible fractionalized excitations in $\alpha - RuCl_3$. *Phys. Rev. Lett.* **114**, 147201 (2015).
15. Banerjee, A. et al. Proximate Kitaev quantum spin liquid behaviour in a honeycomb magnet. *Nature materials* **15**, 733–740 (2016).

16. Do, S.-H. et al. Majorana fermions in the Kitaev quantum spin system α-rucl 3. *Nature Physics* **13**, 1079–1084 (2017).
17. Baek, S.-H. et al. Evidence for a field-induced quantum spin liquid in α-$RuCl_3$. *Phys. Rev. Lett.* **119**, 037201 (2017).
18. Zheng, J. et al. Gapless spin excitations in the field-induced quantum spin liquid phase of $\alpha - RuCl_3$. *Phys. Rev. Lett.* **119**, 227208 (2017).
19. Cao, G. et al. Evolution of magnetism in the single-crystal honeycomb iridates $(Na_{1-x}Li_x)_2IrO_3$. *Phys. Rev. B* **88**, 220414 (2013).
20. Manni, S. et al. Effect of isoelectronic doping on the honeycomb-lattice iridate A_2IrO_3. *Phys. Rev. B* **89**, 245113 (2014).
21. Chaloupka, J., Jackeli, G. & Khaliullin, G. Zigzag magnetic order in the iridium oxide Na_2IrO_3. *Phys. Rev. Lett.* **110**, 097204 (2013).
22. Yamaji, Y. et al. Clues and criteria for designing a Kitaev spin liquid revealed by thermal and spin excitations of the honeycomb iridate Na_2IrO_3. *Phys. Rev. B* **93**, 174425 (2016).
23. Xu, C., Feng, J., Xiang, H. & Bellaiche, L. Interplay between Kitaev interaction and single ion anisotropy in ferromagnetic CrI_3 and $CrGeTe_3$ monolayers. *npj Comput. Mater.* 4 (2018).
24. Xu, C. et al. Possible Kitaev quantum spin liquid state in 2D materials with $S = 3/2$. *Phys. Rev. Lett.* **124**, 087205 (2020).
25. Stavropoulos, P. P., Liu, X. & Kee, H.-Y. Magnetic anisotropy in spin-3/2 with heavy ligand in honeycomb Mott insulators: Application to CrI_3. *Phys. Rev. Res.* **3**, 013216 (2021).
26. Liu, H. & Khaliullin, G. Pseudospin exchange interactions in d^7 cobalt compounds: Possible realization of the Kitaev model. *Phys. Rev. B* **97**, 014407 (2018).
27. Sano, R., Kato, Y. & Motome, Y. Kitaev-Heisenberg hamiltonian for high-spin d^7 Mott insulators. *Phys. Rev. B* **97**, 014408 (2018).
28. Liu, H., Chaloupka, Jcv & Khaliullin, G. Kitaev spin liquid in 3*d* transition metal compounds. *Phys. Rev. Lett.* **125**, 047201 (2020).
29. Baskaran, G., Mandal, S. & Shankar, R. Exact results for spin dynamics and fractionalization in the Kitaev model. *Phys. Rev. Lett.* **98**, 247201 (2007).
30. Baskaran, G., Sen, D. & Shankar, R. Spin-*S* Kitaev model: Classical ground states, order from disorder, and exact correlation functions. *Phys. Rev. B* **78**, 115116 (2008).
31. Chandra, S., Ramola, K. & Dhar, D. Classical Heisenberg spins on a hexagonal lattice with Kitaev couplings. *Phys. Rev. E* **82**, 031113 (2010).
32. Oitmaa, J., Koga, A. & Singh, R. R. P. Incipient and well-developed entropy plateaus in spin-*S* Kitaev models. *Phys. Rev. B* **98**, 214404 (2018).
33. Koga, A., Tomishige, H. & Nasu, J. Ground-state and thermodynamic properties of an $S = 1$ Kitaev model. *J. Phys. Soc. Jpn.* **87**, 063703 (2018).
34. Rousochatzakis, I., Sizyuk, Y. & Perkins, N. B. Quantum spin liquid in the semiclassical regime. *Nat. Commun.* **9**, 1–11 (2018).
35. Dong, X.-Y. & Sheng, D. N. Spin-1 Kitaev-Heisenberg model on a honeycomb lattice. *Phys. Rev. B* **102**, 121102 (2020).
36. Lee, H.-Y., Kawashima, N. & Kim, Y. B. Tensor network wave function of $S = 1$ Kitaev spin liquids. *Phys. Rev. Research* **2**, 033318 (2020).
37. White, S. R. Density matrix formulation for quantum renormalization groups. *Phys. Rev. Lett.* **69**, 2863 (1992).
38. White, S. R. Density-matrix algorithms for quantum renormalization groups. *Phys. Rev. B* **48**, 10345 (1993).
39. Wang, F. & Vishwanath, A. Z_2 spin-orbital liquid state in the square lattice Kugel-Khomskii model. *Phys. Rev. B* **80**, 064413 (2009).
40. Natori, W. M. H., Andrade, E. C., Miranda, E. & Pereira, R. G. Chiral spin-orbital liquids with nodal lines. *Phys. Rev. Lett.* **117**, 017204 (2016).
41. Natori, W. M. H., Daghofer, M. & Pereira, R. G. Dynamics of a $j = \frac{3}{2}$ quantum spin liquid. *Phys. Rev. B* **96**, 125109 (2017).
42. Natori, W. M. H., Andrade, E. C. & Pereira, R. G. SU(4)-symmetric spin-orbital liquids on the hyperhoneycomb lattice. *Phys. Rev. B* **98**, 195113 (2018).
43. Yao, H., Zhang, S.-C. & Kivelson, S. A. Algebraic spin liquid in an exactly solvable spin model. *Phys. Rev. Lett.* **102**, 217202 (2009).
44. Chua, V., Yao, H. & Fiete, G. A. Exact chiral spin liquid with stable spin Fermi surface on the kagome lattice. *Physical Review B* **83**, 180412 (2011).
45. Yao, H. & Lee, D.-H. Fermionic magnons, non-abelian spinons, and the spin quantum hall effect from an exactly solvable spin-1/2 Kitaev model with SU(2) symmetry. *Phys. Rev. Lett.* **107**, 087205 (2011).
46. de Carvalho, V. S., Freire, H., Miranda, E. & Pereira, R. G. Edge magnetization and spin transport in an SU(2)-symmetric Kitaev spin liquid. *Phys. Rev. B* **98**, 155105 (2018).
47. Chulliparambil, S., Seifert, U. F. P., Vojta, M., Janssen, L. & Tu, H.-H. Microscopic models for Kitaev's sixteenfold way of anyon theories. *Phys. Rev. B* **102**, 201111 (2020).
48. de Farias, C. S., de Carvalho, V. S., Miranda, E. & Pereira, R. G. Quadrupolar spin liquid, octupolar kondo coupling, and odd-frequency superconductivity in an exactly solvable model. *Phys. Rev. B* **102**, 075110 (2020).
49. Seifert, U. F. P. et al. Fractionalized fermionic quantum criticality in spin-orbital Mott insulators. *Phys. Rev. Lett.* **125**, 257202 (2020).
50. Natori, W. M. H. & Knolle, J. Dynamics of a two-dimensional quantum spin-orbital liquid: Spectroscopic signatures of fermionic magnons. *Phys. Rev. Lett.* **125**, 067201 (2020).
51. Ray, S. et al. Fractionalized quantum criticality in spin-orbital liquids from field theory beyond the leading order. *Phys. Rev. B* **103**, 155160 (2021).
52. Chulliparambil, S., Janssen, L., Vojta, M., Tu, H.-H. & Seifert, U. F. P. Flux crystals, majorana metals, and flat bands in exactly solvable spin-orbital liquids. *Phys. Rev. B* **103**, 075144 (2021).
53. Burnell, F. J. & Nayak, C. SU(2) slave fermion solution of the Kitaev honeycomb lattice model. *Phys. Rev. B* **84**, 125125 (2011).
54. Knolle, J., Bhattacharjee, S. & Moessner, R. Dynamics of a quantum spin liquid beyond integrability: The Kitaev-Heisenberg-Γ model in an augmented parton mean-field theory. *Phys. Rev. B* **97**, 134432 (2018).
55. Lieb, E. H. Flux phase of the half-filled band. *Phys. Rev. Lett.* **73**, 2158–2161 (1994).
56. Jin, H.-K., Tu, H.-H. & Zhou, Y. Efficient tensor network representation for Gutzwiller projected states of paired fermions. *Phys. Rev. B* **101**, 165135 (2020).
57. Jin, H.-K., Tu, H.-H. & Zhou, Y. Density matrix renormalization group boosted by Gutzwiller projected wave functions. *Phys. Rev. B* **104**, L020409 (2021).
58. Wu, Y.-H., Wang, L. & Tu, H.-H. Tensor network representations of parton wave functions. *Phys. Rev. Lett.* **124**, 246401 (2020).
59. Zhang, S.-S., Halász, G. B., Zhu, W. & Batista, C. D. Variational study of the Kitaev-Heisenberg-Gamma model. *Phys. Rev. B* **104**, 014411 (2021).

Acknowledgements

F. P. acknowledges the support of the Deutsche Forschungsgemeinschaft (DFG, German Research Foundation) under Germany's Excellence Strategy EXC-2111-390814868 and TRR 80. H.-K. J. is funded by the European Research Council (ERC) under the European Unions Horizon 2020 research and innovation program (grant agreement No. 771537). W. M. H. N. and J. K. acknowledge the support from the Royal Society via a Newton International Fellowship through project NIF\R1\181696.

Author contributions

H.-K.J., W.M.H.N., F.P., and J.K. contributed to conception, execution, and write-up of this project. The numerical simulations were performed by H.-K.J.

Funding

Open Access funding enabled and organized by Projekt DEAL.

Competing interests

The authors declare no competing interests.

Additional information

Supplementary information The online version contains supplementary material available at https://doi.org/10.1038/s41467-022-31503-0.

Correspondence and requests for materials should be addressed to Hui-Ke Jin.

Peer review information *Nature Communications* thanks Yasir Iqbal, Hongjun Xiang, and the other, anonymous, reviewer for their contribution to the peer review of this work.

Reprints and permission information is available at http://www.nature.com/reprints

Publisher's note Springer Nature remains neutral with regard to jurisdictional claims in published maps and institutional affiliations.

Open Access This article is licensed under a Creative Commons Attribution 4.0 International License, which permits use, sharing, adaptation, distribution and reproduction in any medium or format, as long as you give appropriate credit to the original author(s) and the source, provide a link to the Creative Commons license, and indicate if changes were made. The images or other third party material in this article are included in the article's Creative Commons license, unless indicated otherwise in a credit line to the material. If material is not included in the article's Creative Commons license and your intended use is not permitted by statutory regulation or exceeds the permitted use, you will need to obtain permission directly from the copyright holder. To view a copy of this license, visit http://creativecommons.org/licenses/by/4.0/.

© The Author(s) 2022